BNL-77062-2006-JA

Available online at www.sciencedirect.com
ScienceDirect
Aerosol Science 38 (2007) 352–369

Journal of
Aerosol Science
www.elsevier.com/locate/jaerosci

Numerical advection of moments of the particle size distribution in Eulerian models

Douglas L. Wright Jr*

2106 Forrest Haven Boulevard, Edison, NJ 08817, USA

Received 6 September 2006; received in revised form 28 November 2006; accepted 30 November 2006

Abstract

'Invalid moment sets'—sets of quantities nominally moments but for which no underlying distribution could exist and therefore not moment sets—are generated in Eulerian models from valid sets by independent advection of each moment. Examination of invalid set generation by two representative advection schemes in one dimension for ensembles of 10^4 test cases spanning a range of initial moment sets and flow velocities reveals invalid set frequencies $\geqslant 0.7\%$ for both schemes. Standard moment methods cannot accommodate invalid sets. Solutions to this problem are presented and evaluated for the ensembles and accurate moment advection free of invalid sets was obtained for both schemes. A new closure scheme insensitive to invalid sets using Lagrange interpolation of moment equation kernels is described and evaluated for condensation, dry deposition, and gravitational settling and found to match the high accuracy of quadrature.

Keywords: Moment methods; Advection of moments; Transport of moments; Stieltjes moment problem; Quadrature method of moments

1. Introduction

Aerosol evolution must be represented in a variety of spatially gridded models, such as the chemical transport and general circulation models used in air quality and climate change studies. These models solve partial differential equations for chemical and aerosol fields $C(x, y, z, t)$ defined at grid box centers (x_i, y_j, z_k) for box (i, j, k). Common to these models is representation of gaseous and particulate emissions, advection, convection, diffusion, surface deposition due to winds, gravity and precipitation, chemical reactions, and aerosol microphysical processes. Process operators (modules) are executed sequentially at each integration step. The aerosol microphysical module represents particle formation from gaseous precursors, gas–particle mass transfer, coagulation, and particle-phase reactions, and from the point of view of module developers the model is a 'host' imposing constraints on aerosol representation and module design. Numerous modules based on the flexible and efficient moments method tracking 2–6 moments have been implemented in such hosts (Ackermann et al., 1998; Binkowski & Roselle, 2003; Binkowski & Shankar, 1995; Easter et al., 2004; Herzog, Weisenstein, & Penner, 2004; Riemer, Vogel, Vogel, & Fiedler, 2003; Wilson, Cuvelier, & Raes, 2001; Wright, Kasibhatla, McGraw, & Schwartz, 2001; Wright, McGraw, Benkovitz, & Schwartz, 2000; Yu et al., 2003).

* Tel.: +1 908 380 7430.
E-mail address: dwright@bnl.gov.

0021-8502/$ - see front matter © 2007 Elsevier Ltd. All rights reserved.
doi:10.1016/j.jaerosci.2006.11.011

For any real number k the Stieltjes moments of size distribution $f(x)$ and size coordinate x (radius, diameter, volume, mass, etc.) are

$$\mu_k = \int_0^\infty x^k f(x)\,\mathrm{d}x \tag{1}$$

and normalized moments are $\bar{\mu}_k = \mu_k/\mu_0$. Necessary and sufficient conditions for existence of a (non-unique) $f(x)$ for moment sequence $k = 0, 1, \ldots, 2l+1$ are non-negative Hankel–Hadamard determinants (Shohat & Tamarkin, 1963):

$$\Delta_{m,l} = \begin{vmatrix} \mu_m & \mu_{m+1} & \cdots & \mu_{m+l} \\ \mu_{m+1} & \mu_{m+2} & \cdots & \mu_{m+l+1} \\ \vdots & \vdots & \vdots & \vdots \\ \mu_{m+l} & \mu_{m+l+1} & \cdots & \mu_{m+2l} \end{vmatrix} \geqslant 0 \tag{2}$$

with $m = 0, 1$; $l \geqslant 0$; $\Delta_{m,l} = 0$ for a monodisperse distribution. Necessary but insufficient is non-negative curvature of $\ln \mu_k$ as a function of k (Feller, 1971): $\mu_k \mu_{k-2} - \mu_{k-1}^2 \geqslant 0$ for all k. Two-moment sets always satisfy Eq. (2). Larger sets violating Eq. (2) inequalities are 'invalid'.

Host models are computationally intensive and consequently of limited spatial resolution, typically 1–500 km. Higher-order advection schemes are therefore essential to minimize numerical diffusion. Polynomials typically approximate trace chemical and particle ('tracer') concentrations between box centers for rows of 1–5 boxes. These schemes, which provide accurate transport of independent tracers, were not designed to preserve tracer interrelationships such as those within moment sets and a 'moment advection problem' arises. The strong spatial and temporal variation of atmospheric aerosols, as well as steep gradients (as may result from a burst of nucleation in a single grid box due to the extreme nonlinearity of the nucleation rate with respect to controlling variables), contributes to this problem. Although any mixing process can potentially generate invalid sets, the present study is limited to advection.

Recent studies (Fan, Marchisio, & Fox, 2004; Settumba & Garrick, 2004; Upadhyay & Ezekoye, 2006) examined size-dependent transport of particle populations represented with moments in the context of computational fluid dynamics (CFD). The present study concerns the passive flow of particle populations with air masses and involves flow velocities (winds) independent of particle size. This is a first investigation of a problem emerging as moment methods tracking more than 2–3 moments per population are developed for atmospheric hosts.

Section 2 characterizes generation of invalid moment sets by two advection schemes representative of those in host models. The remainder of this study is largely independent of the process giving rise to invalid sets. Section 3 discusses the impact of invalid sets on moment methods. Section 4 describes and evaluates several solutions to the moment advection problem, solutions that augment advection schemes when applied to moments (Section 4.1), advect surrogate quantities for moments (Section 4.2), replace or correct invalid sets (Section 4.3), or use closure methods for the moment equations insensitive to invalid sets (Section 4.4). Section 5 contains a summary and concluding remarks.

2. Generation of invalid moment sets

The continuity equation for passive tracer flow in carrier fluid (air) of density ρ and velocity $\mathbf{v}$ with tracer concentration C and mixing ratio $R = C/\rho$ is

$$\frac{\partial(\rho R)}{\partial t} = -\nabla \cdot (\mathbf{v}\rho R) \tag{3}$$

and for the carrier fluid is

$$\frac{\partial \rho}{\partial t} = -\nabla \cdot (\mathbf{v}\rho). \tag{4}$$

With ρ and C defined at box centers, tracer spatial profiles $C(s)$ or $R(s)$ spanning one or more boxes are typically constructed and the equations solved by finite differencing. For a uniform one-dimensional grid with box length L, the contents of segment ΔL of the upstream box will flow into the downstream box during an advective step.

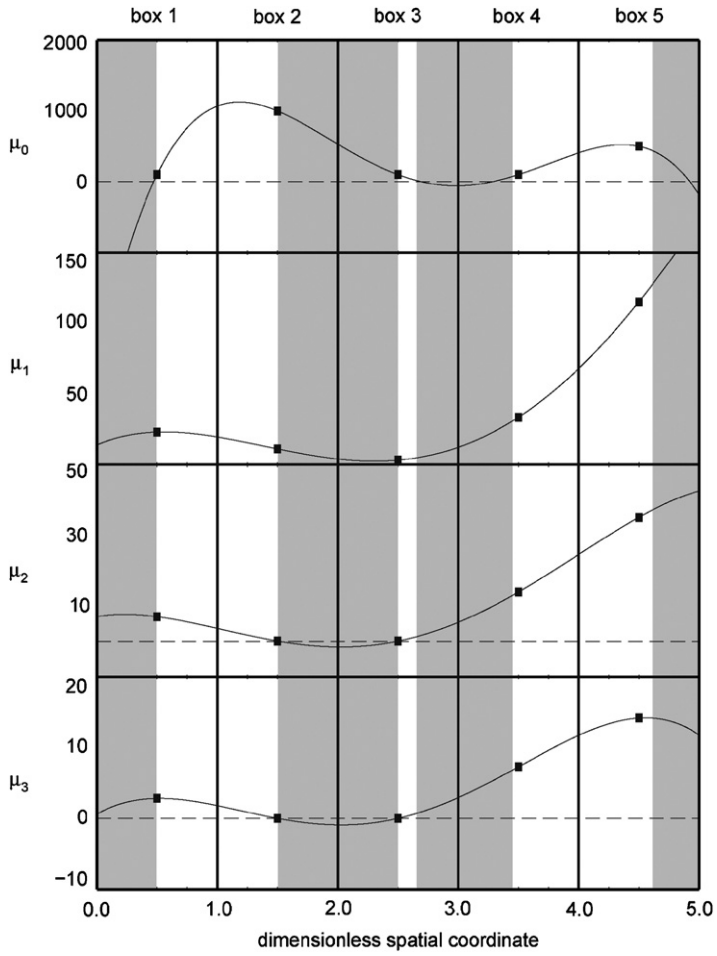

Fig. 1. Quartic polynomial spatial profiles of diameter moments $\mu_k(\mu m^k\,cm^{-3})$ as an illustration of profiles characteristic of some higher-order advection schemes. The μ_k values at the five box centers (filled squares) define the unique quartic for each k and are those of lognormal distributions with parameters $[N(cm^{-3}),\ d_g(\mu m),\ \sigma_g\ (1)]$ set to [100, 0.2, 1.7], [1000, 0.01, 1.6], [100, 0.03, 1.5], [100, 0.3, 1.6], and [500, 0.2, 1.7] for boxes 1–5, respectively, and form valid moment sets at each box center. Invalid moment sets exist at all locations within shaded regions.

Simple (zeroth-order) upstream advection of moments assumes flat (constant) profiles in each box and integration over ΔL multiplies each moment by ΔL. As the inequalities of Eq. (2) are independent of moment normalization, if the box-mean moments form a valid set, so do the moments integrated over ΔL. After the advective step, the box-mean moments in the downstream box will be a weighted average of the moments from ΔL of the upstream box and the moments of the segment of the downstream box remaining in the box over the step. With initial box-mean moments of the downstream box also a valid set, the updated moments of the box will be a weighted average of two valid sets and thus a valid set. No moment advection problem arises with the simple upstream scheme. Unfortunately, it is much too diffusive to be of use in atmospheric hosts.

Higher-order schemes typically use quadratic to quintic profiles ranging over one or more boxes. Fig. 1 shows a set of quartic profiles of diameter ($x = d$) moments $\{\mu_0, \mu_1, \mu_2, \mu_3\}$ passing through the (valid) moment sets at the five box centers defining the polynomial. Steep gradients result in negative concentrations along segments of profiles that positive-definite schemes fill to arbitrary small values or otherwise remove. Steep gradients also produce ratios of tracers that are quite different from those at box centers. Imagine how the ratio of two tracers might vary along a coordinate if one had negative segments filled while the other remained positive without fills—as for the ratios μ_2/μ_0 and μ_3/μ_0 of Fig. 1 with negative segments filled. In Fig. 1 invalid sets exist at each location (within shaded regions) for which any profile was negative as well as within two segments (near the center of box 4 and most of the right-hand

portion of box 5) where all profiles are positive. As with the ratio of two tracers at a specific location, the ratio of the advected amounts of two tracers within ΔL can be quite different from ratios at the centers of the upstream and downstream boxes. For the profiles of Fig. 1 and with ρ uniform and $\Delta L = L/2$ for all boxes, the contents of the right-hand side of box 2 are advected into box 3 during an integration step and the advected amounts of μ_2 and μ_3 are arbitrarily small while that of μ_0 is significant. Thus the ratios μ_2/μ_0 and μ_3/μ_0 for the advected segment are very different from those of the valid sets at the two box centers. Also, integration of each moment over the right-hand side (ΔL) of box 2 yields an invalid set, as does similar integration over the left-hand side of box 3, and the updated moment set of box 3 after the step is the sum of these two invalid sets and (in this instance) an invalid set (two invalid sets can sum to a valid set). Thus, any required moment interrelationships that obtain at the two box centers prior to the advective step need not be preserved when the downstream box-mean concentrations are updated.

Generation of invalid moment sets was examined for two advection schemes using uniform flow velocities in one dimension. If invalid sets are not produced in one dimension they will not appear in three dimensions with the common x–y–z operator splitting. Tracer *spatial* moments $G_l = \int s^l C(s)\,\mathrm{d}s$ are useful in describing these schemes.

The Bott (1989a, 1989b) scheme solves Eq. (3) by constructing an nth order polynomial profile spanning $2n+1$ boxes and renormalizing tracer fluxes. It is positive definite and conserves the zeroth spatial tracer moment. The computer code was derived from that of the multiscale air quality simulation platform (Odman & Ingram, 1996). Fourth-order polynomials were used inside the domain, and second- and then first-order near the boundaries.

The second-order (*spatial*) moments method of Prather (1986), or the quadratic upstream scheme (QUS), jointly solves Eqs. (3) and (4). It conserves zeroth-, first-, and second-order spatial tracer moments using quadratic profiles in each box independent of other boxes with discontinuities across box boundaries. The computer code was derived from that of the Goddard Institute of Space Studies general circulation model downloaded from http://www.giss.nasa.gov/tools/modelE. Fluxes were limited as in Prather (1986) to ensure smooth positive-definite profiles without fills.

Generation of invalid sets in the presence of steep gradients is now illustrated. Initial diameter moments $\{\mu_0, \mu_1, \mu_2, \mu_3\}$ were those of lognormal distributions with number concentration $N(\mathrm{cm}^{-3})$, geometric mean diameter $d_g(\mu\mathrm{m})$, and geometric standard deviation σ_g (1). For a 20-box model, initial moments were those for (N, d_g, σ_g) set to (10^6, 0.01, 1.5) for box 3, (10^4, 0.2, 1.8) for box 4, and (10^3, 0.03, 1.8) for all other boxes. The spatially uniform fraction $F = \Delta L/L$ was set to 0.15. After each of 96 advective steps and for each box in which $\mu_0 \geqslant 0.1\,\mathrm{cm}^{-3}$ (a threshold applied for all statistics) necessary and sufficient conditions $\mu_2\mu_0 - \mu_1^2 \geqslant 0$ and $\mu_3\mu_1 - \mu_2^2 \geqslant 0$ were tested. For the Bott scheme, 29% of the sets were invalid and for the QUS, 5.4%. Fig. 2a shows initial profiles and Fig. 2b profiles after 70 steps. The higher-order nature of the Bott scheme is apparent.

The frequency of occurrence of invalid sets was determined for an ensemble of 10^4 test cases systematically covering a wide range of initial moments sets and flow velocities. Three sets of lognormal distributions were defined. For the first set, 10 evenly spaced (log scale) values of N on the interval $[10^{-1}, 10^5]$, 10 evenly spaced (log scale) values of d_g on the interval [0.01, 0.04], and 10 evenly spaced (linear scale) values of σ_g on the interval [1.1, 2.0] were selected and a product space grouping yielded 10^3 distinct distributions. A second set of 10^3 distributions was similarly obtained where N spanned $[10^{-1}, 10^4]$, d_g spanned [0.04, 0.16], and σ_g values were as in set 1. For a third set N spanned $[10^{-1}, 10^3]$, d_g spanned [0.16, 0.50], and σ_g values were again as in set 1. With these sets of distributions 10^3 distinct assignments of initial moments for a 60-box model were made, where the mth assignment took moments of the mth distribution of set 1 for box 3, moments of the mth distribution of set 2 for box 4, and moments of the mth distribution of set 3 for all other boxes. Each of the 10^3 assignments was combined with each of 10 evenly spaced (linear scale) values of F on the interval [0.05, 0.95] to provide 10^4 test cases. Forty-eight advective steps yielded $10^4 \times 60 \times 48 = 2.88 \times 10^7$ moment sets tested against the two inequalities given in the preceding paragraph. Although the moment set in each box is initially that of a unimodal lognormal distribution, moment sets of multimodal distributions arise at locations of spatial gradients as the differing moment sets in adjacent boxes are mixed during update of the moment set for each box. For the Bott scheme, 3.8% of the sets were invalid and for the QUS, 0.70%. The ensemble average of the number of invalid sets present increased as integration proceeded with both schemes. If larger univariate or multivariate moment sets were tracked instead of the simple 4-moment set considered here, greater invalid set frequencies would have resulted as such moment sets must satisfy a larger number of inequalities and are thus more liable to invalidation.

Three-moment models such as those with lognormal (N, d_g, σ_g) determined from moments are common and statistics on invalid subsets were obtained for $\{\mu_0, \mu_1, \mu_2\}$, $\{\mu_0, \mu_1, \mu_3\}$, and $\{\mu_0, \mu_2, \mu_3\}$. These subsets are valid if $\bar{\mu}_2 - \bar{\mu}_1^2 \geqslant 0$, $\bar{\mu}_3 - \bar{\mu}_1^3 \geqslant 0$, and $\bar{\mu}_3 - \bar{\mu}_2^{3/2} \geqslant 0$, respectively. Bott scheme (QUS) invalid subset frequencies (%) were 2.5 (0.35), 2.5 (0.30), and 2.3 (0.31) , respectively, less than the 4-moment frequencies but still considerable.

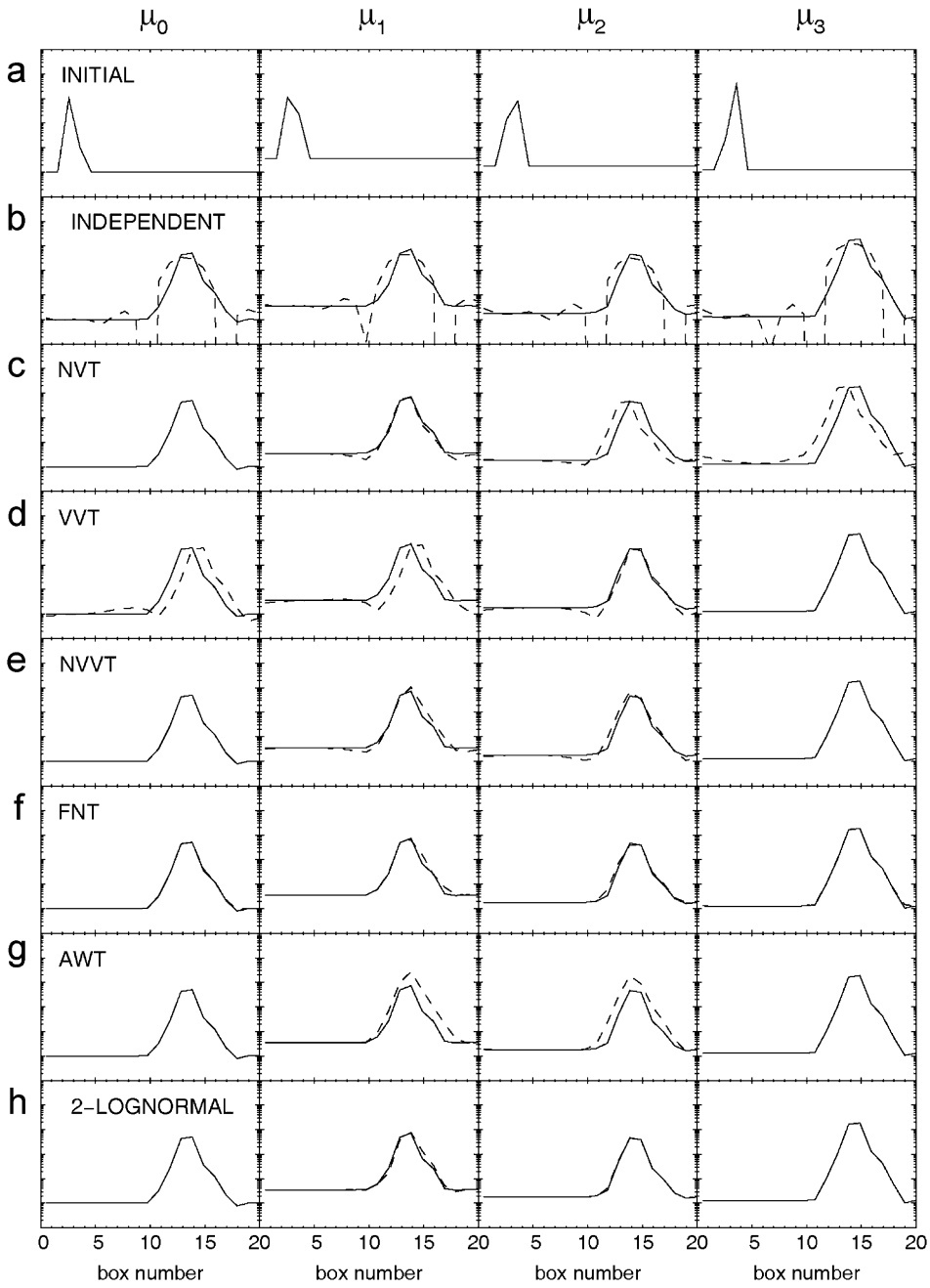

Fig. 2. Spatial profiles of diameter moments μ_k (μm^k cm^{-3}) for an illustrative case described in Section 2. Panel (a) shows initial profiles and all other panels show profiles after 70 advective steps. In panels (b)–(h), solid lines are profiles obtained by independent advection of each moment with the Quadratic Upstream Scheme (QUS). Dashed lines in (b) are profiles obtained by independent advection of each moment with the Bott scheme. Dashed lines in (c)–(h) are profiles obtained with the QUS in conjunction with (c) number vector transport (NVT, Section 4.1), (d) volume vector transport (VVT, Section 4.1), (e) number–volume vector transport (NVVT, Section 4.1), (f) fixed-node transport (FNT, Section 4.2.1), (g) abscissa-weight transport (AWT, Section 4.2.2), and (h) a 2-lognormal replacement scheme (Section 4.3). Ordinates are log-scale and span $[10^2, 10^8]$ for μ_0, $[10^0, 10^6]$ for μ_1, $[10^{-1}, 10^5]$ for μ_2, and $[10^{-2}, 10^4]$ for μ_3.

Statistics were also obtained for variant ensembles having reduced gradients. An ensemble with the d_g ranges of the three sets of lognormals reduced to [0.05, 0.10], [0.10, 0.15], and [0.15, 0.20], respectively, and all σ_g set to 1.8 yielded decreased (4-moment) invalid set frequencies of 0.63% (Bott) and 0.0023% (QUS). An ensemble without gradients in

either d_g or σ_g (and thus normalized moments) yielded no invalid sets with either scheme. These results confirm the role of gradients in the production of invalid moment sets.

These model experiments characterize invalid moment set generation by advection. Diffusion and convection can also give rise to invalid sets. If advection alone produced invalid sets, their subsequent mixing with valid ones could propagate further invalid sets or restore validity to those sets, depending upon the amount of aerosol represented by an invalid set and the degree to which necessary inequalities were violated. Aerosol sources such as injection of particles into the model domain and particle formation from gaseous precursors are represented by new valid sets and tend to restore (validity to) invalid sets upon mixing. Sinks remove valid and invalid sets alike. The impact of advection-generated invalid sets on the aerosol moment fields is likely to be highly host-dependent.

A thought experiment suggests that if generation of invalid sets were sufficiently infrequent it might be viewed as a local, transient problem. A host (with three spatial dimensions) is initialized with valid sets and large gradients in normalized moments. In absence of sources, sinks, and boundary fluxes, mixing through transport eventually leads to a stationary, well-mixed state. The spatial distribution of moment sets in this state would be that obtained by summing all moment sets over the domain—thus forming a single domain-sum (valid) set—and assigning the normalized moments of that domain-sum set to all boxes and apportioning the domain sum of the normalizing moment (number, etc.) over boxes in proportion to the quantity of air (carrier fluid) in a box. Any production of invalid sets at locales of steep gradients during early stages of mixing notwithstanding, as the well-mixed state is approached all moment sets tend toward valid ones.

3. Invalid moment sets and moment methods

Invalid sets pose fundamental mathematical problems for moment methods. Moment evolution equations

$$\frac{\mathrm{d}\mu_k}{\mathrm{d}t} = \int P_k(x) f(x)\,\mathrm{d}x + \int\!\!\int Q_k(x, y) f(x) f(y)\,\mathrm{d}x\,\mathrm{d}y \tag{5}$$

are solved with $P_k(x)$ the kernel for one particle processes such as condensation, dry deposition, and gravitational settling and $Q_k(x, y)$ the kernel for coagulation. The right-hand side can be expressed directly in terms of known moments only in special cases—the closure problem.

Closure methods are herein classified into four types. Type 1 methods assume a distribution functional form with evolution of its time-dependent parameters determined by evolution of moments (Binkowski & Roselle, 2003; Pratsinis, 1988; Whitby & McMurry, 1997). Type 2 methods assume a functional form for moments in terms of the moment index k (Barrett & Jheeta, 1996) or otherwise interpolate moments needed for closure (Frenklach & Harris, 1987). Type 3 methods use quadrature (McGraw, 1997; Barrett & Webb, 1998; McGraw & Wright, 2003; Marchisio & Fox, 2005), and Type 4 methods assume alternate functional forms for the kernels of Eq. (5) (Section 4.4, Terry, McGraw, & Rangel, 2001). Type 2 and Type 4 methods are free of invalid moment set concerns and will be taken up in Section 4.4. The relative merits of the various closure methods are not discussed here other than with respect to the moment advection problem under consideration.

Type 1 methods typically use lognormal or modified gamma distributions. Any two normalized moments ($k > 0$) fix a lognormal σ_g, e.g., $\ln \sigma_g = [\ln(\bar{\mu}_2/\bar{\mu}_1^2)]^{1/2}$. If the necessary inequality $\bar{\mu}_2 - \bar{\mu}_1^2 \geqslant 0$ is not satisfied, $\ln \sigma_g$ is imaginary. The modified gamma distribution $f(x) = ax^\alpha \exp(-bx^s)$ with a, b, s, and α positive parameters is used in Hulburt and Katz (1964) and Barrett and Webb (1998) with $s = 1$ and $b = \bar{\mu}_1/(\bar{\mu}_2 - \bar{\mu}_1^2)$. If $\bar{\mu}_2 - \bar{\mu}_1^2 \geqslant 0$ is not satisfied, b is negative and $f(x)$ diverges at large x. For any distribution form invalid sets will yield unphysical parameters.

Type 3 methods involve quadrature inversion from $2n$ moments $\{\mu_0, \ldots, \mu_{2n}\}$ to n abscissas $\{x_1, \ldots, x_n\}$ and n weights $\{w_1, \ldots, w_n\}$ satisfying the $2n$ equations

$$\mu_k = \sum_{i=1}^{n} x_i^k w_i. \tag{6}$$

Any integral property Π of the distribution with kernel $p(x)$ can then be approximated as

$$\Pi = \int p(x) f(x)\,\mathrm{d}x \cong \sum_{i=1}^{n} p(x_i) w_i. \tag{7}$$

The x_i can be interpreted as particle sizes (diameters, volumes, etc.) and the w_i as concentrations (number, etc.) so all x_i and w_i must be non-negative. Solutions to Eq. (6) with non-negative x_i and w_i do not exist for invalid sets for if such a solution $\{x_1, \ldots, x_n, w_1, \ldots, w_n\}$ were to exist it would constitute an n-disperse distribution satisfying Eq. (1). This difficulty arises for the quadrature method of moments (QMOM, McGraw, 1997) in its original form for which inversions are required at each integration step of Eq. (5). The Jacobian matrix transformation form of the QMOM (McGraw & Wright, 2003) and the direct quadrature method of moments (DQMOM, Marchisio & Fox, 2005) directly track abscissas and weights rather than moments and avoid explicit inversions and moment set validity concerns. For the same tracked moments in a unit volume both forms of the QMOM and the DQMOM are equivalent. The transported quantities for the DQMOM are not moments and their use in atmospheric hosts is discussed in Section 4.2.

4. Solutions to the moment advection problem

Solutions to the moment advection problem are now presented. Desiderata are (1) ease of implementation, aided by advecting moments in like manner as other tracers, (2) permitting quantification of errors associated with solution of this problem, (3) incorporation within the aerosol module and thus independence of host characteristics, (4) applicability for arbitrary sets of integral properties including multivariate moment sets, and (5) requiring a minimal number of tracers.

Solutions were evaluated using two standards of reference. Moment sets obtained with each solution were compared with sets obtained by independent advection of each moment ('independent-advection reference' hereinafter). This provides a measure of how well the accuracy of an advection scheme designed for transport of independent tracers is maintained when the scheme is coupled to techniques preserving moment set validity. Such evaluations are to some extent independent of the accuracy of the advection scheme itself and therefore relevant when the solutions are coupled to other advection schemes. Moment sets obtained with each solution were also compared with exact results obtained by uniform translation of initial moment profiles downstream ('exact reference' hereinafter). The independent-advection moment sets were also compared with the exact results. For each standard of reference and each k, the ratio R_k of the larger to the smaller of the solution and reference μ_k values was geometrically averaged over all ensemble test cases, grid boxes, and advective steps and unity subtracted to obtain a measure of error E_k symmetric with respect to over- and underestimation (Benkovitz & Schwartz, 1997). Table 1 shows E_k values for each solution examined, and the average value of E_k over the moment set is included as a measure of overall solution accuracy. The E_k values obtained for solutions coupled to the Bott scheme were somewhat sensitive to the choice of the arbitrary small value used to replace zero concentrations. With this scheme, a lower bound of 10^{-10} was applied after each advective step, taken as the smallest physically significant value of any of the moments in the set $\{\mu_0, \mu_1, \mu_2, \mu_3\}$, and calculated as the value of μ_3 for a population of particles each of 1-nm diameter and having the threshold number concentration ($0.1\,\mathrm{cm}^{-3}$). Decreasing the lower bound to 10^{-20} increased the E_k values, but had little impact on the relative accuracy among the various solutions. The intent of this study was to evaluate approaches to moment advection for each advection scheme in its own right, and proximate statements of solution errors for the two schemes are not intended to suggest comparison of the advection schemes themselves.

4.1. Augmented advection schemes for moment sets—vector transport

Any advection scheme can be augmented to avoid generation of invalid sets while leaving treatment of other tracers unchanged. Four steps describe the approach. Operator splitting in x, y, and z is assumed and one dimension is discussed; without operator splitting implementation is more complicated.

First, choose a normalizing moment. If moments of the number distribution are modeled μ_0 is the natural (but not only) choice and is assumed in describing steps 2–4. Second, normalize all other tracked integral aerosol properties Π (moments, chemical concentrations, etc.) by μ_0 to obtain intensive properties $\bar{\Pi}$. Third, advect μ_0 in like manner as other tracers and store its fluxes. Fourth, use the fluxes and initial μ_0 values to determine the fractional contributions f_{i-1}, f_i, and f_{i+1} ($f_{i-1} + f_i + f_{i+1} = 1$) of boxes $i-1$, i, and $i+1$ to the updated μ_0 of box i. All intensive properties are then updated as

$$\bar{\Pi}(t + \Delta t) = f_{i-1}\bar{\Pi}_{i-1}(t) + f_i\bar{\Pi}_i(t) + f_{i+1}\bar{\Pi}_{i+1}(t). \tag{8}$$

Table 1
Error statistics for solutions to the moment advection problem for the ensemble of 10^4 test cases

Solutions with the Bott scheme	$E_{0,\mathrm{Bott}}$	$E_{1,\mathrm{Bott}}$	$E_{2,\mathrm{Bott}}$	$E_{3,\mathrm{Bott}}$	E_{ave}	$E_{0,\mathrm{exact}}$	$E_{1,\mathrm{exact}}$	$E_{2,\mathrm{exact}}$	$E_{3,\mathrm{exact}}$	E_{ave}
Number vector transport	0.000	0.066	0.137	0.252	0.114	0.660	0.431	0.327	0.374	0.448
Volume vector transport	0.163	0.097	0.045	0.000	0.076	0.746	0.446	0.309	0.354	0.464
Number-volume vector transport	0.000	0.115	0.128	0.000	0.061	0.660	0.492	0.426	0.504	0.521
Fixed-node transport (a)	0.041	0.046	0.059	0.103	0.062					
Fixed-node transport (b)	0.059	0.229	0.228	0.133	0.163	0.689	0.638	0.500	0.420	0.562
Abscissa-weight transport	0.001	0.097	0.113	0.012	0.056	0.667	0.475	0.394	0.492	0.507
2-lognormal replacement	0.000	0.117	0.107	0.000	0.056	0.660	0.542	0.461	0.504	0.542
1-lognormal replacement	0.000	0.082	0.057	0.000	0.035	0.660	0.521	0.402	0.504	0.522
Independent advection						0.660	0.442	0.364	0.504	0.493
Solutions with the QUS	$E_{0,\mathrm{QUS}}$	$E_{1,\mathrm{QUS}}$	$E_{2,\mathrm{QUS}}$	$E_{3,\mathrm{QUS}}$	E_{ave}	$E_{0,\mathrm{exact}}$	$E_{1,\mathrm{exact}}$	$E_{2,\mathrm{exact}}$	$E_{3,\mathrm{exact}}$	E_{ave}
Number vector transport	0.000	0.055	0.103	0.159	0.079	0.107	0.101	0.133	0.206	0.137
Volume vector transport	0.459	0.216	0.071	0.000	0.186	0.531	0.238	0.095	0.052	0.229
Number-volume vector transport	0.000	0.085	0.080	0.000	0.041	0.107	0.132	0.111	0.053	0.101
Fixed-node transport (a)	0.008	0.008	0.006	0.005	0.007					
Fixed-node transport (b)	0.025	0.180	0.166	0.027	0.099	0.130	0.235	0.201	0.078	0.161
Abscissa-weight transport	0.000	0.066	0.066	0.000	0.033	0.107	0.109	0.094	0.053	0.091
2-lognormal replacement	0.000	0.002	0.002	0.000	0.001	0.107	0.056	0.040	0.053	0.064
1-lognormal replacement	0.000	0.001	0.001	0.000	0.000	0.107	0.055	0.040	0.053	0.064
Independent advection						0.107	0.055	0.040	0.053	0.064

Solutions are described in Section 4. For each moment, the ratio R_k of the larger to the smaller of the solution and reference μ_k values was geometrically averaged over all test cases, grid boxes, and advective steps and unity subtracted to obtain the measure of error E_k. For solutions with the Bott scheme (QUS), E_k values calculated with respect to reference results obtained by independent advection of each moment with the Bott scheme (QUS) are denoted $E_{k,\mathrm{Bott}}$ ($E_{k,\mathrm{QUS}}$), and averages over k are listed as E_{ave}. The E_k values calculated with respect to exact results for advected moments are denoted $E_{k,\mathrm{exact}}$ and averages over k are also listed as E_{ave}. The E_k values calculated for moments obtained by independent advection with respect to exact results are also given. For fixed-node transport, entry (a) contains statistics on the equivalence of advection of moments and advection of surrogate quantities for moments for the variant ensemble described in paragraph 2 of Section 4.2.1; entry (b) contains statistics for the basecase ensemble appropriate for comparison with other solutions and discussed in paragraph 3 of Section 4.2.1.

The $\bar{\Pi}$ are updated as each transport operator is applied and the aerosol module reconstructs the full Π for microphysics. Each normalized property $\bar{\Pi}$ can be viewed as a unit vector in an abstract space with the normalizing moment fixing vector length. Normalization by μ_0 yields 'number vector transport' (NVT) and by μ_3 'volume vector transport' (VVT). As the fourth step averages valid sets, vector transport always yields valid sets.

Profiles obtained with NVT and VVT in conjunction with the QUS are shown in Fig. 2c and d for the 20-box illustration described in Section 2. Both NVT and VVT profiles show a phase error relative to profiles obtained by independent transport of each moment, an error that increases with the magnitude of the difference between the moment index k and the index of the normalizing moment. Ensemble statistics are shown in Table 1. Trends in E_k with k are consistent with errors visible in Fig. 2 for NVT and VVT. Both methods conserved domain sums of moments with errors solely in spatial distribution. For the Bott scheme, VVT matched the independent-advection reference more closely than NVT, but for the QUS the converse was true. A degree of anticorrelation between number concentration and particle size in the ensemble (and atmosphere) tends to yield lesser gradients in higher-order moments than in lower-order ones, and lesser gradients in μ_3 than in μ_0 might account for the better accuracy of the μ_3-normalized VVT relative to the μ_0-normalized NVT with the Bott scheme.

NVT coupled with VVT and transforms preserving moment set validity yielded a 'number-volume vector transport' (NVVT) scheme with independent advection of μ_0 and μ_3. Fig. 3 accompanies the NVVT procedure now described. An NVT advective step yields normalized moments $\bar{\mu}_k^{\mathrm{NVT}}$ and moments $\mu_k^{\mathrm{NVT}}(\mathrm{B})$ while a concurrent VVT step with a distinct moment set yields $\bar{\mu}_k^{\mathrm{VVT}}$ and $\mu_k^{\mathrm{VVT}}(\mathrm{C})$. In this illustration NVT overestimates moments 1, 2, and 3 while VVT underestimates moments 0, 1, and 2 relative to reference $\mu_k(\mathrm{A})$. Rescaling $\mu_k^{\mathrm{NVT}}(\mathrm{B})$ by $[\mu_3(\mathrm{A})/\mu_3^{\mathrm{NVT}}(\mathrm{B})]^{k/3}$ yields $\mu_k^{\mathrm{NVT}}(\mathrm{D})$ and leaves μ_0^{NVT} unchanged and forces $\mu_3^{\mathrm{NVT}}(\mathrm{D})$ to match $\mu_3(\mathrm{A})$. This rescaling is mathematically equivalent to changing moment units from $\mu\mathrm{m}^k\,\mathrm{cm}^{-3}$ to $\delta^k\,\mathrm{cm}^{-3}$ for δ a suitably chosen length scale and preserves

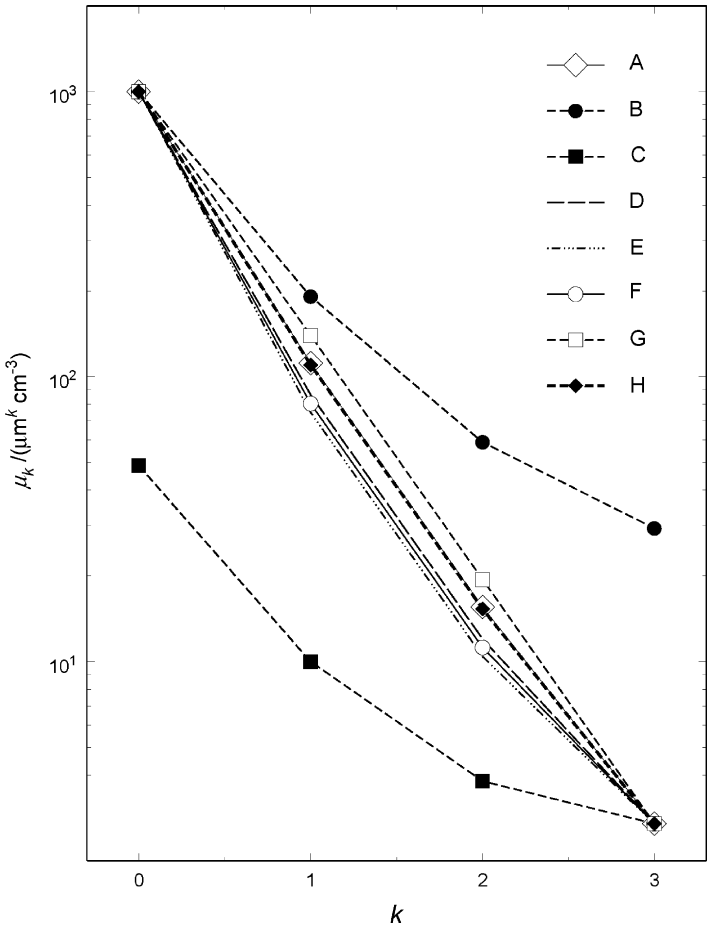

Fig. 3. Illustration of the number–volume vector transport (NVVT) scheme (Section 4.1). After a number vector transport (NVT) advective step yields the moments of curve B and a concurrent volume vector transport (VVT) step with a distinct moment set yields the moments of curve C, a sequence of transforms that preserve moment set validity leads to the moments of curve H as an approximation to the reference moments of curve A. The transforms are described in the text. The moments of curves F and G were averaged with equal weighting for this illustration.

set validity. Similarly, rescaling $\mu_k^{\mathrm{VVT}}(\mathrm{C})$ by $[\mu_0(\mathrm{A})/\mu_0^{\mathrm{VVT}}(\mathrm{C})]^{(3-k)/3}$ yields $\mu_k^{\mathrm{VVT}}(\mathrm{E})$ and leaves μ_3^{VVT}unchanged and forces $\mu_0^{\mathrm{VVT}}(\mathrm{E})$ to match $\mu_0(\mathrm{A})$. The $\mu_k^{\mathrm{NVT}}(\mathrm{D})$ and $\mu_k^{\mathrm{VVT}}(\mathrm{E})$ are then averaged to yield $\mu_k^{\mathrm{NVVT}}(\mathrm{F})$. Tests showed $\mu_1^{\mathrm{NVVT}}(\mathrm{F})$ and $\mu_2^{\mathrm{NVVT}}(\mathrm{F})$ biased low. Moments $\mu_k^{\mathrm{mono}}(\mathrm{G})$ of the monodisperse distribution with number concentration $\mu_0(\mathrm{A})$ and volume concentration $\pi\mu_3(\mathrm{A})/6$ are constructed and a weighted average of $\mu_k^{\mathrm{NVVT}}(\mathrm{F})$ (85%) and $\mu_k^{\mathrm{mono}}(\mathrm{G})$ (15%) removes most of the bias and yields the (final) NVVT moments $\mu_k^{\mathrm{NVVT}}(\mathrm{H})$.

Profiles obtained with NVVT in conjunction with the QUS are shown in Fig. 2e for the 20-box illustration of Section 2 and ensemble statistics are shown in Table 1. With respect to the independent-advection reference, overall NVVT accuracy was greater than that of NVT or VVT for both advection schemes. With respect to the exact reference, NVVT coupled to the QUS was again more accurate than NVT or VVT, but coupled to the Bott scheme, solution errors were dominated by those in the advection scheme itself and consequently all vector transport schemes showed similar accuracy. NVVT does not precisely conserve domain sums of μ_1 and μ_2. For each test case the ratio $R_{k,\mathrm{domain}} = \sum \mu_k(\mathrm{final})/\sum \mu_k(\mathrm{initial})$ was calculated and for each k the geometrical average $\bar{R}_{k,\mathrm{domain}}$ over all test cases is shown in Table 2.

NVT extended to include diffusion and convection has been implemented for 6-moment sets in three hosts: the global chemistry model driven by observation-derived meteorology (Wright et al., 2000) employing a variant (Easter, 1993) of the Bott scheme, the multiscale air quality simulation platform (Yu et al., 2003) employing the Bott (1989a,

Table 2
Conservation statistics for domain sums of μ_1 and μ_2 for the ensemble of 10^4 test cases for solutions not precisely conserving these domain sums

Solution method	$\bar{R}_{1,\text{domain}}$	$\bar{R}_{2,\text{domain}}$
Bott		
Number–volume vector transport	0.981	1.006
Abscissa–weight transport	1.135	1.082
2-lognormal replacement	0.924	0.963
1-lognormal replacement	0.963	0.975
QUS		
Number–volume vector transport	0.916	0.967
Abscissa–weight transport	1.126	1.098
2-lognormal replacement	0.993	0.996
1-lognormal replacement	0.996	1.000

For each test case the ratio $R_{k,\text{domain}} = \sum \mu_k(\text{final}) / \sum \mu_k(\text{initial})$ was calculated along with its ensemble geometrical average $\bar{R}_{k,\text{domain}}$.

1989b) scheme, and a host employing the semi-Lagrangian scheme of Lin and Rood (1996), which does not fully split into one-dimensional operators. Each implementation required reverse engineering of the computer code for each host transport process. A desire to avoid this considerable host-specific task initiated the present search for more easily implemented means of moment transport.

Vector transport is very efficient when there are a large number of tracked variables per particle population since each normalized variable $\bar{\Pi}$ is updated with few operations [Eq. (8)] once the normalizing moment has been transported—bin sectional modules requiring transport of one to several variables for each of eight or more size bins for each of several populations could benefit greatly. Vector transport also directly extends to multivariate moment sets and other properties (e.g., concentrations of multiple chemical components) for which normalization by the transported moment is appropriate. For schemes storing several quantities for each tracer advected, such as the QUS with its nine spatial moments per tracer (in three-dimensional applications), the reduced number of tracers required by vector transport greatly reduces storage requirements.

4.2. Transport of surrogate quantities for moments

Representing moments with independent extensive quantities during transport precludes generation of invalid sets. Simple upstream advection of the quantities $\xi_{j,i}$ for box i can be expressed as

$$\xi_{j,i}(t+\Delta t) = c_{i-1}\xi_{j,i-1}(t) + c_i\xi_{j,i}(t) + c_{i+1}\xi_{j,i+1}(t) \tag{9}$$

with the c_i the same for all tracers. If the $\mu_{k,i}$ could be expressed as linear functions of the $\xi_{j,i}$ with coefficients $h_{k,j}$ then

$$\begin{aligned}\mu_{k,i}(t+\Delta t) &= \sum_j h_{k,j}\xi_{j,i}(t+\Delta t) = \sum_j h_{k,j}[c_{i-1}\xi_{j,i-1}(t) + c_i\xi_{j,i}(t) + c_{i+1}\xi_{j,i+1}(t)] \\ &= c_{i-1}\sum_j h_{k,j}\xi_{j,i-1}(t) + c_i\sum_j h_{k,j}\xi_{j,i}(t) + c_{i+1}\sum_j h_{k,j}\xi_{j,i+1}(t) \\ &= c_{i-1}\mu_{k,i-1}(t) + c_i\mu_{k,i}(t) + c_{i+1}\mu_{k,i+1}(t)\end{aligned} \tag{10}$$

and transport of the $\xi_{j,i}$ would be equivalent to transport of the $\mu_{k,i}$. Moment transport through non-negative independent extensive surrogates ξ_j (dropping the box index i) relies on this equivalence even with higher-order advection schemes. This equivalence is examined in Section 4.2.1. The ξ_j are transformed to μ_k for microphysical calculations. Three types of surrogate transport for moments are now described, although only the first relies on Eq. (10).

4.2.1. Fixed-node transport

For n moments and n fixed 'nodes' a set of n constant intensive quantities $\{\bar{\rho}_{k,j}\}$ for each node j can be defined such that the moments are linear functions of n extensive coefficients $\{\xi_j\}$

$$\mu_k = \sum_{j=1}^{n} \xi_j \bar{\rho}_{k,j} \tag{11}$$

with ξ_j a number (volume, etc.) concentration and $\{\bar{\rho}_{k,j}\}$ a normalized 'basis' moment set for node j that is the same for all grid boxes in the host domain. For diameter moments a simple choice is $\bar{\rho}_{k,j} = d_j^k$, the normalized moments of a monodisperse distribution of diameter d_j. For $n = 2$ the set $\{\bar{\rho}_{k,j}\}$ can be chosen to permit exact solution of Eq. (11) for the ξ_j, but for larger n a set $\{\bar{\rho}_{k,j}\}$ permitting exact solution with $\xi_j \geqslant 0$ for all occurring sets $\{\mu_k\}$ does not exist. With $n = 4$ and d_j logarithmically spanning [0.01, 1.0] μm, nodes are spaced by a factor of $100^{1/3} = 4.64$ and moments of narrow distributions lying entirely between two adjacent nodes cannot be exactly represented. In such cases a non-linear search can locate a set $\{\xi_j\}$ approximately yielding the μ_k for chosen $\bar{\rho}_{k,j}$.

The assumed equivalence of surrogate and moment advection was examined for 'fixed-node transport' (FNT) and a variant ensemble. Each initial moment set $\{\mu_k\}$ of the original ensemble was transformed to a set of number concentrations $\{\xi_j\}$ with $\bar{\rho}_{k,j} = d_j^k$ and d_j spanning [0.01, 1.4] μm. Initial ξ_j for non-linear searches were obtained by (exact) solution of Eq. (11), taking the absolute value of each ξ_j, and rescaling each $|\xi_j|$ by $\mu_0 / \sum_j |\xi_j|$. Searches minimized

$$\sum_{k=0}^{3} \left[q_k \left(\sum_{j=1}^{n} (\xi_j^{1/2})^2 \bar{\rho}_{k,j} - \mu_k \right) \Big/ \mu_k \right]^2 \tag{12}$$

with respect to $\xi_j^{1/2}$ to yield positive-definite $\xi_j = (\xi_j^{1/2})^2$ with weightings q_k for $k = \{0, 1, 2, 3\}$ set to {0.35, 0.15, 0.15, 0.35}. As moments $\mu_k(\xi_j)$ calculated from Eq. (11) with retrieved ξ_j did not exactly match the μ_k of the original ensemble, independent-advection reference results for the variant ensemble were obtained using the $\mu_k(\xi_j)$ as initial moments. Ensemble statistics are shown in Table 1. Moments obtained with FNT and the QUS gave E_k values relative to the variant reference of 0.5–0.8%, showing near equivalence of fixed-node surrogate advection and direct advection of moments. FNT with the Bott scheme gave E_k values of 4–10%. Domain sums of moments were conserved ($\bar{R}_{k,\text{domain}} = 0$) with FNT with both schemes.

Profiles obtained with FNT in conjunction with the QUS are shown in Fig. 2f for the 20-box illustration of Section 2. FNT was also evaluated for the original ensemble for comparison with other solutions despite differences in initial moments when non-linear searches were required. Non-linear searches were required for 97% of the ensemble initial moment sets and yielded average errors of 1–2% in μ_0 and μ_3 and 14–17% in μ_1 and μ_2. Ensemble statistics are shown in Table 1. With the Bott scheme, FNT accuracy with respect to both references was less than that of all other solutions, but mitigating factors in atmospheric hosts will be discussed below. Similarly with the QUS, FNT accuracy was less than that of all other solutions except VVT.

FNT permits transport of surrogates in like manner as other tracers, implementation within the aerosol module, and quantification of $\mu_k \rightarrow \xi_j$ transform errors when non-linear searches are done. It is applicable for any integral property for which a suitable basis set can be defined. The computational burden of non-linear searches can be greatly reduced (and possibly eliminated) through precalculated lookup tables (see Section 4.4 for table design) providing accurate initial guesses for the ξ_j for each possible moment set. The FNT inaccuracies shown in Table 1 for the ensemble are mitigated in atmospheric hosts by three factors. First, new particles from nucleation and particulate emissions would enter hosts at node sizes and thus permit (in absence of other processes) exact $\mu_k \leftrightarrow \xi_j$ transforms. Second, after transport, and after the exactly solvable $\xi_j \rightarrow \mu_k$ transform is done in preparation for microphysical evolution of the μ_k, slow evolution through coagulation at ambient particle concentrations would (in absence of other processes) permit the subsequent $\mu_k \rightarrow \xi_j$ transform to be accurate. Third, rapid condensational growth of small particles would likely be the greatest source of narrow between-node distributions and errors associated with non-linear searches, but recent parameterizations (Kerminen & Kulmala, 2002; Kerminen, Anttila, Lehtinen, & Kulmala, 2004) of small-particle dynamics potentially eliminate the need to explicitly model early growth of new particles. Evaluation in hosts with all process operators active would be especially informative with FNT.

4.2.2. Abscissa-weight transport

For $2n$ moments the DQMOM requires transport of quadrature weights $\{w_1, \ldots, w_n\}$ and weighted abscissas $\{w_1x_1, \ldots, w_nx_n\}$, independent extensive quantities yielding valid moment sets through Eq. (6). In a CFD context, Marchisio and Fox (2005) emphasize terms ("C_α" therein) in transport equations for the w_i and w_ix_i that depend upon diffusion coefficients and gradients in x_i, terms essential if transport of the w_i and w_ix_i is to be equivalent to transport of moments. Moments can be rapidly obtained from the w_i and w_ix_i for microphysical evolution, and this approach to transport can be used in conjunction with aerosol modules using any type of moment method.

The construction of C_α-type terms appropriate for the processes and operator structure of atmospheric hosts has not been investigated. As a variant of the DQMOM approach, an 'abscissa-weight transport' (AWT) scheme neglecting C_α-type terms was defined and evaluated. For diameter moments $\{\mu_0, \mu_1, \mu_2, \mu_3\}$ surrogate quantities $\{w_1, w_2\}$ and $\{w_1d_1^3, w_2d_2^3\}$ are advected, chosen for accurate transport of μ_0 and μ_3. After each advective step abscissas are obtained as $d_i = [(w_id_i^3)/w_i]^{1/3}$ and then μ_1 and μ_2 from Eq. (6).

Profiles obtained with AWT in conjunction with the QUS are shown in Fig. 2g for the 20-box illustration of Section 2. The large errors visible for μ_1 and μ_2 are not representative of overall AWT accuracy. Ensemble statistics are shown in Table 1. With both advection schemes, the accuracy of AWT with respect to both references was similar to that of NVVT, and was better than that of NVT or VVT except for the Bott scheme with respect to the exact reference. Domain sums of μ_1 and μ_2 were on average $\sim 10\%$ too high (Table 2) with AWT for both advection schemes. Small errors in μ_0 and μ_3 with respect to the independent-advection reference were a result of the fact that advection of a total quantity in two parts followed by summation is not precisely equivalent to advection of the single total quantity.

AWT permits transport of surrogates in like manner as other tracers, incorporation within the aerosol module, and easy implementation through quadrature inversions for modules evolving moments—the inverted moment sets are produced within the module and thus valid. Extension to multivariate moment sets is possible provided appropriate multivariate inversions can be devised (Wright, McGraw, & Rosner, 2001; McGraw & Wright, 2003). The AWT scheme evaluated here uses one advected tracer per tracked moment and thus requires at least twice as many tracers as equally accurate but more difficult to implement NVVT.

4.2.3. Alternative integral properties to moments and weakly constrained moment sets

Consider the set $\{\mu_0, \gamma_1, \gamma_2, \mu_3\}$ with γ_1 and γ_2 defined as the integrals of the smooth kernels $g_1(x)$ and $g_2(x)$ over the size distribution. Choosing $g_k(x)$ as x^k yields the $k = 0$–3 moments. Do alternative choices of $g_k(x)$ exist such that the resulting set is free of or only weakly subject to intraset constraints such as those of Eq. (2) for moments? If so an aerosol model might be built for the quantities $\{\mu_0, \gamma_1, \gamma_2, \mu_3\}$. Evolution equations for the γ_k would be obtained in like manner as those for the μ_k, i.e. by multiplying the aerosol general dynamic equation by $g_k(x)$ and integrating over x. The resulting integrals over the size distribution could be approximated via Eq. (7) using a quadrature solving the nonlinear system (assumed solvable) consisting of Eq. (6) for μ_0 and μ_3 and Eq. (7) for γ_1 and γ_2. Alternatively, the transform (assumed possible) $\{\mu_0, \gamma_1, \gamma_2, \mu_3\} \rightarrow \{\mu_0, \mu_1, \mu_2, \mu_3\}$could be made (with perhaps as intermediary the quadrature $\{w_1, w_2, x_1, x_2\}$ obtained as just described), the moment equations integrated, and the inverse transform done. If this stratagem were feasible it could yield an integral-property aerosol model transporting independent quantities free of intraset constraints. 'Integral' here implies that $g_k(x)$ is not extremely narrow for otherwise a size-resolved model results. The alternative set might represent the aerosol as effectively as moments for retrieval of the optical properties important in atmospheric hosts.

Even if the parenthetic assumptions above were valid this stratagem would not likely succeed. With number concentration (μ_0) and mean volume ($\pi\mu_3/6\mu_0$) fixed, it is difficult to identify smooth functions $g_k(x)$ that yield unconstrained properties γ_k. A first tracked moment specifies the quantity of aerosol present. A second normalized by the first yields a first intensive property. Additional intensive properties (defined as ratios of extensive properties) of the size spectrum will not be independent of the first. Thus intraset constraints are not unique to moments but exist within any set of three or more integral quantities where each quantity is obtained from a smooth kernel.

Smoothness of the kernels $g_k(x)$ results in overlap of the integrands $g_k(x)f(x)$ which in turn gives rise to intraset constraints—i.e. properties of one (distinct) portion of the size spectrum impose no constraint upon those of another. This suggests that integrand overlap can be reduced and constraints weakened by appropriate selection of tracked integral properties. The moment integrands $x^k f(x)$—for which larger particles become increasingly important as k increases—show less overlap as spacing of the k-values increases—e.g., the volume distribution overlaps the number distribution less than it does the surface area distribution. Weakening of intraset constraints was examined for a sequence

of 3-moment sets $\{\mu_0, \mu_1, \mu_n\}$, $n = 2$–9, using additional variant (wrt the moments tracked) ensembles and the QUS. The validity condition for each set is $\bar{\mu}_n - \bar{\mu}_1^n \geqslant 0$. For $n = 2, 3, 4, 5, 6, 7, 8$ and 9 the frequency (%) of invalid sets was 0.35, 0.30, 0.19, 0.091, 0.069, 0.061, 0.050 and 0.042, showing the anticipated reduction in frequency. If invalid sets were simply to be replaced upon detection (Section 4.3), consideration of integrand overlap could assist selection of favorable moment sets for tracking.

4.3. Replacement or correction of invalid moment sets

Invalid moment sets generated by any model process can be replaced by similar valid ones upon detection. A '2-lognormal' scheme preserving μ_0 and μ_3 was evaluated for the ensemble and the set $\{\mu_0, \mu_1, \mu_2, \mu_3\}$. The subsets $\{\mu_0, \mu_1, \mu_3\}$ and $\{\mu_0, \mu_2, \mu_3\}$ fixed (N, d_g, σ_g) for two lognormals whose moments were averaged to provide a replacement set. Lognormal σ_g's were confined to [1.05, 3.0] to handle invalid subsets and improve accuracy. Invalid sets were replaced at each occurrence and the simulation resumed.

Profiles obtained with the 2-lognormal scheme in conjunction with the QUS are shown in Fig. 2h for the 20-box illustration of Section 2. Ensemble statistics are shown in Table 1. Errors (E_k) in μ_1 and μ_2 with respect to the independent-advection reference were 11% for the Bott scheme and 0.2% for the QUS. Domain sums of μ_1 and μ_2 were not precisely conserved and $\bar{R}_{k,\text{domain}}$ values are shown in Table 2.

The community multiscale air quality (CMAQ) modeling system is a widely used research and regulatory host incorporating a Type 1 moment module tracking $\{\mu_0, \mu_2, \mu_3\}$ (Binkowski & Roselle, 2003). It uses a lognormal replacement scheme preserving μ_0 and μ_3 and confining σ_g to [1.05, 2.5] by adjusting μ_2 for invalid or unphysical moment sets. Ensemble statistics for this '1-lognormal' scheme with μ_1 derived from the replacement lognormal are shown in Table 1. The accuracy of the 1-lognormal scheme (with respect to the independent-advection reference) slightly exceeded that of the 2-lognormal scheme for both advection schemes. Gradients tend to increase with decreasing moment index (Section 4.1) and steeper gradients in μ_1 than in μ_2 may account for the greater accuracy of 1-lognormal replacement using only $\{\mu_0, \mu_2, \mu_3\}$ than 2-lognormal replacement with its additional $\{\mu_0, \mu_1, \mu_3\}$ subset. Errors (E_2) in μ_2 (with respect to the independent-advection reference) for the Bott scheme (QUS) were 6% (0.1%).

The lognormal replacement schemes tracked independent moment advection more closely than any other solution for both advection schemes. They are trivial to implement and make quantifiable adjustments to moment sets, statistical measures of which are easily obtainable in hosts.

If an advection scheme yields invalid sets as a result of severe inaccuracies in only 1 or 2 moments, those moments can be identified as outliers in the moment sequence through difference tables and corrected while leaving other moments in the set unchanged. This is attractive for sets consisting of a sequence of ~ 6 or more moments for which outliers can be effectively identified. Details are given in McGraw (2006).

Replacement or corrected sets can displace invalid sets or be used solely to obtain right-hand sides of moment equations and derivative (e.g., optical) properties. The latter use imposes no spurious perturbation on the set (and thus domain sums) and allows subsequent transport and mixing to (potentially) restore set validity.

4.4. Closure methods insensitive to invalid moment sets

Many individual moments or ratios of moments represent important aerosol properties in their own right independent of membership in a set. Moment fields largely accurate but not free of invalid sets might be acceptable if (1) assessment of net aerosol influence (climate change, air quality) is the goal, (2) replacement of invalid sets in calculation of optical properties is satisfactory, and (3) microphysical evolution can be modeled.

Moment methods exist that do not rely upon the existence of an underlying distribution and consequently have no particular sensitivity to moment set validity. For $2n$ moments, Barrett and Jheeta (1996) took $\ln \mu_k$ as a polynomial of order $2n-1$ in moment index k to interpolate moments needed for closure. Polynomial fitting in k does not require valid sets. Barrett and Jheeta (1996) found that higher-order polynomials improve accuracy over the quadratic (lognormal) approximation. Kernels for one particle processes must be representable as $P_k(x) = \sum_j a_{k,j} x^{\alpha_j}$ with $a_{k,j}$ and α_j real numbers.

Atmospheric hosts require kernels spanning the full size spectrum for condensation, coagulation, wind-driven (dry) deposition and gravitational settling, kernels not exactly representable in this form. This section presents a new closure scheme fitting these kernels with the α_j necessarily restricted to the k-values of the moment set tracked, but the method

of Barrett and Jheeta (1996) with arbitrary real α_j offers greater flexibility in fitting the kernels and merits further exploration in light of the moment advection problem.

A closure scheme insensitive to invalid sets was devised using Lagrange polynomial interpolation (LI, Press, Teukolsky, Vetterling, & Flannery, 1992) of the kernels. This is in contrast to Type 2 approaches, which interpolate moments. For $P_k(x) = \sum_{j=0}^{2n-1} a_{k,j} x^j$ exact for $2n$ selected values of x evenly spaced on the interval $[x_L, x_U]$ the $2n$ moment equations $d\mu_k/dt = \sum_{j=0}^{2n-1} a_{k,j} \mu^j$ are closed. The points x_L and x_U are determined solely from tracked moments. A LI scheme was examined in box-model calculations for (1) accuracy with appropriate x_L and x_U provided, (2) sensitivity to x_L and x_U, and (3) determination of x_L and x_U when invalid sets are potentially present.

LI and QMOM accuracies were compared for condensation and combined deposition and settling in radius space ($x = r$) for $n = 2, 3$ with the $2n$ selected values of r logarithmically spaced and r_L and r_U taken as the smallest and largest quadrature abscissas from inversion of the (here valid) LI moment set. Moments of a superposition of three lognormal modes of varying (N, r_g, σ_g) provided initial sets for each of 27 test cases constructed by product space grouping as in Section 2. Kernels and test cases are described in the Appendix. For condensation, LI polynomials (obtained with aid of the *polcof* routine of Press et al., 1992) were updated at each integration step as the distribution advances through size space; for deposition and settling the polynomials were constant. Highly accurate results for moment evolution were obtained with a discrete distribution model with 5000 particle sizes for condensation and 1000 for deposition and settling. Each case simulated a 24-h period. The magnitude of relative error was averaged over all integration steps, test cases, and $2n$ moments to yield error measures $E_{QMOM}(\%)$ and $E_{LI}(\%)$; results are presented as (n, E_{QMOM}, E_{LI}). For condensation the measures were (2, 0.094, 0.093) and (3, 0.030, 0.030) and for deposition and settling (2, 1.8, 1.8) and (3, 1.2, 1.3). Thus, suitable r_L and r_U give the LI scheme the accuracy of quadrature for these kernels.

Sensitivity of LI accuracy to r_L and r_U was examined with variant simulations in which $r_U$was taken as 1.2 times the largest abscissa and r_L the smallest abscissa divided by 1.2. Deposition and settling gave measures (2, 1.8, 1.0) and (3, 1.2, 1.0), showing increased LI accuracy. Condensation sometimes yielded narrow distributions for which $r_U \cong r_L$; consequently, imposing $r_U/r_L > 1.2^2$ created spurious errors that invalidated this test. Errors should decrease with time as the distribution narrows yet in some cases grew rapidly toward the end of the integration. Thus the measures obtained, (2, 0.094, 0.72) and (3, 0.030, 0.43), at best indicate upper limits on the sensitivity of the LI scheme to r_L and r_U for condensation.

If LI is to offer a solution to the moment advection problem, it must not rely upon quadrature inversions to obtain r_L and r_U during host execution, as invalid sets are not invertible. For the small moment sets (3–6 moments) most important for atmospheric hosts, r_L and r_U can be robustly provided by precalculated lookup tables. For $n = 2$ and with $\bar{\mu}_0$ unity, $\bar{\mu}_1$, $\bar{\mu}_2$, and $\bar{\mu}_3$ can serve as continuous indices to tables $\mathbf{T}_L$ and $\mathbf{T}_U$ of r_L and r_U. Moment interrelationships lead to an irregular table design as now described. For $\bar{\mu}_1$ a range $[\bar{\mu}_{1,\min}, \bar{\mu}_{1,\max}]$ was set to [0.01, 1.0] μm and 100 log-spaced values $\bar{\mu}_{1,i}$ were defined. For each $\bar{\mu}_{1,i}$ a range $[\bar{\mu}_{2,i,\min}, \bar{\mu}_{2,i,\max}]$ was set to $[1.01\bar{\mu}_{1,i}^2, 11.3\bar{\mu}_{1,i}^2]$ and 50 (log-spaced) values $\bar{\mu}_{2,i,j}$ defined. For each $\bar{\mu}_{1,i}$ and $\bar{\mu}_{2,i,j}$ a range $[\bar{\mu}_{3,i,j,\min}, \bar{\mu}_{3,i,j,\max}]$ was set to $[1.01\bar{\mu}_{2,i,j}^2/\bar{\mu}_{1,i}, 11.5\bar{\mu}_{2,i,j}^2/\bar{\mu}_{1,i}]$ and 100 values $\bar{\mu}_{3,i,j,k}$ defined. For each of the $100 \times 50 \times 100$ sets $\{1, \bar{\mu}_{1,i}, \bar{\mu}_{2,i,j}, \bar{\mu}_{3,i,j,k}\}$, r_L and r_U were set to the smaller and larger of the quadrature abscissas and stored in $\mathbf{T}_L$ and $\mathbf{T}_U$. During integration of the moment equations, table indices (I, J, K) for the set $\{1, \bar{\mu}_1, \bar{\mu}_2, \bar{\mu}_3\}$ were identified at each step as

$$I = \mathrm{NINT}[\ln(\bar{\mu}_1/\bar{\mu}_{1,\min})/X_1] + 1,$$

$$J = \mathrm{NINT}[\ln(\bar{\mu}_2/\bar{\mu}_{2,i,\min})/X_2] + 1,$$

$$K = \mathrm{NINT}[\ln(\bar{\mu}_3/\bar{\mu}_{3,i,j,\min})/X_3] + 1 \tag{13}$$

with NINT the nearest integer function and X_1, X_2, and X_3 the constant table spacings in $\ln\bar{\mu}_1$, $\ln\bar{\mu}_2$, and $\ln\bar{\mu}_3$. Indices I and K were limited to [1, 100] and J to [1, 50] as invalid sets produce values outside these ranges, and r_L and r_U were taken as $\mathbf{T}_L(I, J, K)$ and $\mathbf{T}_U(I, J, K)$. For the set of 27 test cases, error measures for condensation were (2, 0.094, 0.13) and for combined deposition and settling (2, 1.8, 1.7). Retrieval of tabular r_L and r_U rather than direct quadrature inversion had little impact on LI accuracy.

These results demonstrate the accuracy of the LI scheme for the processes considered, but further investigation is needed before a comprehensive assessment of the merits of the LI scheme relative to other methods can be made. Straightforward LI for the coagulation double integral requires two-dimensional polynomial forms and is left to future work. Explicit treatment of ultrafine particle dynamics can be avoided in most host applications, and in the absence

of large concentrations of small particles coagulation will be slow and sufficient accuracy likely attainable. Direct extension of LI to 6-moment sets through five-dimensional lookup tables would be demanding of computer memory, but the three-dimensional tables $\mathbf{T}_{\mathrm{L}}(I, J, K)$ and $\mathbf{T}_{\mathrm{U}}(I, J, K)$ indexed with only three normalized moments may be suitable even for larger moment sets.

The QMOM might avoid inversion problems due to invalid sets by retrieving tabular abscissas and weights in like manner as the LI scheme retrieves r_{L} and r_{U}. The success of LI with tabular r_{L} and r_{U} likely depends on its weak sensitivity to r_{L} and r_{U}. QMOM accuracy with moments computed from tabular r_i and w_i as $\mu_k = \sum_{i=1}^{n} r_i^k w_i$ would need evaluation as table resolution is limited by storage requirements.

5. Summary and concluding remarks

Generation of invalid moment sets through independent advection of each moment was characterized in one dimension for two advection schemes representativeve of those in Eulerian atmospheric models. Invalid sets were produced at significant frequencies ($\geqslant 0.7\%$) for both schemes and pose fundamental mathematical problems for standard moment methods. Several solutions to this problem were described and evaluated for ensembles of test cases spanning a wide range of initial moment sets and flow velocities and accurate moment transport was obtained with a number of approaches. A new moment closure scheme insensitive to invalid sets and matching the accuracy of quadrature was presented and evaluated for condensation, dry deposition, and gravitational settling, with extension to coagulation left to future work. A few concluding remarks follow.

Assessment of invalid moment set generation is needed within comprehensive hosts where the mitigating or exacerbating effects of other processes can be included. One-dimensional studies are useful to characterize the problem and examine potential solutions, but the severity of the problem in two- and three-dimensional integrated models requires assessment in each host.

Several criteria useful in assessing the merits of various solutions to the moment advection problem were given in the first paragraph of Section 4. For the implementation of a particular moment-based aerosol module in a particular host, more than one of the solutions examined may be attractive. No one solution is expected to be the optimal choice for every application. The intent of this study was to provide a number of alternatives from which the model builder can choose. If ease of implementation and accuracy are most important, a simple lognormal replacement scheme may be appropriate, and in any event, implementing this scheme first and obtaining statistics to assess the severity of invalid set generation before proceeding to other solutions is perhaps a good starting point.

Easy interchange among variant process (operator) modules is important in atmospheric hosts. Vector and fixed-node transport facilitate this interchange as they are suitable for both moment and bin sectional aerosol modules. For large numbers of aerosol variables with either module type, the efficiency and lesser storage of vector transport may merit the task of implementation.

Two-moment models are always free of invalid sets. Upadhyay and Ezekoye (2003) point out difficulties with 2- and 3-point quadrature for the narrow distributions formed by condensational growth of newly formed particles in aerosol reactors and found the accuracy of the 2-moment 1-point QMOM surprisingly good. The relative merits of tracking n 2-moment sets versus a single $2n$-moment set should be examined for the specific aerosol types represented in atmospheric hosts and the goals of host applications. A $2n$-moment set will have advantages in evolution of size-coordinate aspects, but n 2-moment sets may be preferable when different parts of the size spectrum have different chemical composition.

Minimizing numerical diffusion and preserving moment set validity appear contrary in that the latter suggests transport of the aerosol as a single entity (as in vector transport) while the former is favored by independent advection of each moment. New advection schemes designed to preserve moment interrelationships would permit model builders to utilize the full power of moment methods unhampered by moment set validity concerns, but such schemes may be difficult to devise.

Acknowledgments

The author would like to thank Robert McGraw for innumerable discussions of all things moments and Gary Russell of the NASA Goddard Institute for Space Studies for helpful discussions. Support was provided by U.S. Department

of Energy (DE-AC02-98CH10866). The U.S. Government retains nonexclusive, royalty free license to publish or reproduce the published form of this contribution or to allow others to do so, for U.S. Government purposes.

Appendix A. Kernels for condensation and combined dry deposition and gravitational settling

The condensation kernel for μ_k included the Fuchs–Sutugin transition-regime expression for the particle growth rate ($\mathrm{d}r/\mathrm{d}t$) (derived from Eqs. 12.3 and 11.34 of Seinfeld & Pandis, 1998)

$$P_k^{\mathrm{cond}}(r) = kr^{k-1}\frac{\mathrm{d}r}{\mathrm{d}t} = \frac{kr^{k-2}D}{\rho_{\mathrm{particle}}}\left(\frac{1+Kn}{1+0.377Kn+1.33Kn(1+Kn)/\alpha}\right)(\rho_v - \rho_{v,0}) \tag{A.1}$$

with D the diffusivity of the condensing vapor (treated as H_2SO_4) in air (set to $10^{-5}\,\mathrm{m^2\,s^{-1}}$), ρ_v the vapor concentration (set to $1.63\times10^{-10}\,\mathrm{kg\,m^{-3}}$, equivalent to 10^9 molecules $\mathrm{cm^{-3}}$ and sufficient for rapid particle growth), $\rho_{v,0}$ the vapor concentration at the particle surface (set to zero), ρ_{particle} the particle density (set to $1500\,\mathrm{kg\,m^{-3}}$), Kn the Knudsen number λ_{a}/r with λ_{a} the mean free path of the vapor in air (set to 0.0663 μm), and α the mass accommodation coefficient (set to unity).

The dry deposition kernel for μ_k was

$$P_k^{\mathrm{ddep}}(r) = -r^k v_{\mathrm{d}}(r)/\Delta z \tag{A.2}$$

with Δz the thickness of the lowest vertical layer of the host model (set to 100 m) and $v_{\mathrm{d}}(r)$ the particle deposition velocity ($\mathrm{m\,s^{-1}}$) including gravitational settling. The deposition velocity (Eq. 20.11 of Jacobson, 2005, the source of all subsequent cited equations) was

$$v_{\mathrm{d}}(r) = \frac{1}{R_{\mathrm{a}} + R_b + R_{\mathrm{a}}R_b v_{\mathrm{g}}} + v_{\mathrm{g}} \tag{A.3}$$

with gravitational settling velocity (Eq. 20.4)

$$v_{\mathrm{g}} = \frac{2r^2(\rho_{\mathrm{particle}} - \rho_{\mathrm{a}})g}{9\eta_{\mathrm{a}}}G \tag{A.4}$$

with ρ_{a} the density of air (set to $1.225\,\mathrm{kg\,m^{-3}}$), g the acceleration due to gravity ($\mathrm{m\,s^{-2}}$), η_{a} the dynamic viscosity of air (set to $1.79\times10^{-5}\,\mathrm{kg\,m^{-1}\,s^{-1}}$), and G the Cunningham slip-flow correction (Eq. 15.30)

$$G = 1 + Kn[1.249 + 0.42\exp(-0.87/\mathrm{Kn})]. \tag{A.5}$$

In Eq. (A.3), R_{a} is the aerodynamic resistance ($\mathrm{s\,m^{-1}}$), calculated using Eqs. 20.12 and 8.38 (stable conditions, with $z_{0,q}$ replacing $z_{0,h}$) as

$$R_{\mathrm{a}} = \frac{1}{k_{\mathrm{v}}u^*}\left[Pr_t \ln\frac{z_{\mathrm{r}}}{z_{0,q}} + \frac{\beta_h}{L}(z_{\mathrm{r}} - z_{0,q})\right] \tag{A.6}$$

with k_{v} the von Karman constant (set to 0.4), u^* the friction wind speed (set to $0.15\,\mathrm{m\,s^{-1}}$), Pr_t the turbulent Prandtl number (set to 0.95), z_{r} a reference height (set to the typical value of 10 m), $z_{0,q}$ the surface roughness length (m) for a particle of radius r, calculated as $D_{\mathrm{r}}/(k_{\mathrm{v}}u^*)$ (Eq. 8.13 for particles) with Dr the particle diffusion coefficient ($\mathrm{m^2\,s^{-1}}$)$k_{\mathrm{B}}TG/(6\pi r\eta_{\mathrm{a}})$ (Eq. 15.29) with $T = 298.15$ K, β_h a constant (set to 7.8), and L the Monin–Obukhov length (set to 5 m). The resistance to molecular diffusion R_b ($\mathrm{s\,m^{-1}}$) was calculated as (Eq. 20.14)

$$R_b = \frac{(Sc/Pr)^{2/3}}{k_{\mathrm{v}}u^*}\ln\frac{z_{0,m}}{z_{0,q}} \tag{A.7}$$

with Sc the particle Schmidt number $\eta_{\mathrm{a}}/(\rho_{\mathrm{a}}D_{\mathrm{r}})$, Pr the dimensionless Prandtl number $\eta_{\mathrm{a}}c_{p,m}/\kappa_{\mathrm{a}}$ with $c_{p,m}$ the heat capacity of air (set to $1007\,\mathrm{J\,kg^{-1}\,K^{-1}}$) and κ_{a} the thermal conductivity of air (set to $2.53\times10^{-5}\,\mathrm{W\,m^{-1}\,K^{-1}}$), and $z_{0,m}$ the length scale (m) for momentum taken as $0.11\eta_{\mathrm{a}}/(\rho_{\mathrm{a}}u^*)$ (Eq. (8.9)). The wind speed implicit in this choice of parameters is $9.7\,\mathrm{m\,s^{-1}}$.

Appendix B. Initial moment sets for the test cases of Section 4.4

Initial moments for the 27 test cases were obtained in similar manner to those of the ensemble described in Section 2. Three sets of 27 lognormal distributions each were defined. For the first set, three evenly spaced (log scale) values of N on the interval $[10^3, 10^5]\,\mathrm{cm}^{-3}$, three evenly spaced (log scale) values of r_g on the interval $[0.01, 0.06]\,\mu\mathrm{m}$, and three evenly spaced (linear scale) values of σ_g on the interval $[1.1, 1.6]$ were selected and a product space grouping yielded 27 distinct distributions. A second set was similarly obtained where N spanned $[10^2, 10^3]$, r_g spanned $[0.08, 0.15]$, and σ_g spanned $[1.7, 2.0]$. For a third set N spanned $[10^1, 10^2]$, r_g spanned $[0.2, 0.4]$, and σ_g spanned $[1.2, 1.3]$. Initial moments for the mth test case were those of the superposition of the mth lognormal distribution of each of the three sets.

References

Ackermann, I. J., Hass, H., Memmesheimer, M., Ebel, A., Binkowski, F. S., & Shankar, U. (1998). Modal aerosol dynamics model for Europe: Development and first applications. *Atmospheric Environment*, *32*, 2981–2999.

Barrett, J. C., & Jheeta, J. S. (1996). Improving the accuracy of the moments method for solving the aerosol general dynamic equation. *Journal of Aerosol Science*, *27*, 1135–1142.

Barrett, J. C., & Webb, N. A. (1998). A comparison of some approximate methods for solving the aerosol general dynamic equation. *Journal of Aerosol Science*, *29*, 31–39.

Benkovitz, C. M., & Schwartz, S. E. (1997). Evaluation of modeled sulfate and SO_2 over North America and Europe for four seasonal months in 1986–1987. *Journal of Geophysical Research*, *102*, 25,305–25,338.

Binkowski, F. S., & Roselle, S. J. (2003). Models-3 Community Multiscale Air Quality (CMAQ) model aerosol component 1. Model description. *Journal of Geophysical Research*, *108*, 4183.

Binkowski, F. S., & Shankar, U. (1995). The Regional Particulate Matter Model 1. Model description and preliminary results. *Journal of Geophysical Research*, *100*, 26,191–26,209.

Bott, A. (1989a). A positive definite advection scheme obtained by nonlinear renormalization of the advective fluxes. *Monthly Weather Review*, *117*, 1006–1015.

Bott, A. (1989b). Reply. *Monthly Weather Review*, *117*, 2633–2636.

Easter, R. C. (1993). Two modified versions of Bott's positive-definite numerical advection scheme. *Monthly Weather Review*, *121*, 297–304.

Easter, R. C., Ghan, S. J., Zhang, Y., Saylor, R. D., Chapman, E. G., Laulainen, N. S. et al. (2004). MIRAGE: Model description and evaluation of aerosols and trace gases. *Journal of Geophysical Research*, *109*, D20210.

Fan, R., Marchisio, D. L., & Fox, R. O. (2004). Application of the direct quadrature method of moments to polydisperse gas–solid fluidized beds. *Powder Technology*, *139*, 7–20.

Feller, W. (1971). *An introduction to probability theory and its applications (Vol. II, p. 155)*. New York: Wiley.

Frenklach, M., & Harris, S. J. (1987). Aerosol dynamics modeling using the method of moments. *Journal of Colloid and Interface Science*, *118*, 252–261.

Herzog, M., Weisenstein, D. K., & Penner, J. E. (2004). A dynamic aerosol module for global chemical transport models: Model description. *Journal of Geophysical Research*, *109*, D18202.

Hulburt, H. M., & Katz, S. (1964). Some problems in particle technology: A statistical mechanical formulation. *Chemical Engineering Science*, *19*, 555–574.

Jacobson, M. Z. (2005). *Fundamentals of atmospheric modeling*. New York: Cambridge.

Kerminen, V.-M., Anttila, T., Lehtinen, K. E. J., & Kulmala, M. (2004). Parameterization for atmospheric new-particle formation: Application to a system involving sulfuric acid and condensable water-soluble organic vapors. *Aerosol Science and Technology*, *38*, 1001–1008.

Kerminen, V.-M., & Kulmala, M. (2002). Analytical formulae connecting the "real" and the "apparent" nucleation rate and the nuclei number concentration for atmospheric nucleation events. *Journal of Aerosol Science*, *33*, 609–622.

Lin, S.-J., & Rood, R. B. (1996). Multidimensional flux-form semi-Lagrangian transport schemes. *Monthly Weather Review*, *124*, 2046–2070.

Marchisio, D. L., & Fox, R. O. (2005). Solution of population balance equations using the direct quadrature method of moments. *Journal of Aerosol Science*, *36*, 43–73.

McGraw, R. (1997). Description of aerosol dynamics by the quadrature method of moments. *Aerosol Science and Technology*, *27*, 255–265.

McGraw, R. (2006). Correcting moment sequences for errors associated with advective transport. ⟨http://www.ecd.bnl.gov/pubs/momentcorrection_mcgraw2006.pdf⟩.

McGraw, R., & Wright, D. L. (2003). Chemically resolved aerosol dynamics for internal mixtures by the quadrature method of moments. *Journal of Aerosol Science*, *34*, 189–209.

Odman, M. T., & Ingram, C. L. (1996). Technical report: Multiscale air quality simulation platform (MAQSIP): Source code documentation and validation, *Rep. ENV-96TR002-v1.0*, 83 pp., MCNC Environmental Programs, Research Triangle Park, NC.

Prather, M. J. (1986). Numerical advection by conservation of second-order moments. *Journal of Geophysical Research*, *91*, 6671–6681.

Pratsinis, S. E. (1988). Simultaneous nucleation, condensation, and coagulation in aerosol reactors. *Journal of Colloid and Interface Science*, *124*, 416–427.

Press, W. H., Teukolsky, S. A., Vetterling, W. T., & Flannery, B. P. (1992). *Numerical Recipes in FORTRAN*. Cambridge: Cambridge University Press.

Riemer, N., Vogel, H., Vogel, B., & Fiedler, F. (2003). Modeling aerosol on the mesoscale-γ: Treatment of soot aerosol and its radiative effects. *Journal of Geophysical Research*, *108*, 4601.

Seinfeld, J. H., & Pandis, S. N. (1998). *Atmospheric chemistry and physics*. New York: Wiley.

Settumba, N., & Garrick, S. C. (2004). A comparison of diffusive transport in a moment method for nanoparticle coagulation. *Journal of Aerosol Science*, *35*, 93–101.

Shohat, J. A., & Tamarkin, J. D. (1963). *The problem of moments*. Providence, RI: American Mathematical Society.

Terry, D. A., McGraw, R., & Rangel, R. H. (2001). Method of moments solutions for a laminar flow aerosol reactor model. *Aerosol Science and Technology*, *34*, 353–362.

Upadhyay, R. R., & Ezekoye, O. A. (2003). Evaluation of the 1-point quadrature approximation in QMOM for combined aerosol growth laws. *Journal of Aerosol Science*, *34*, 1665–1683.

Upadhyay, R. R., & Ezekoye, O. A. (2006). Treatment of size-dependent aerosol transport processes using quadrature based moment methods. *Journal of Aerosol Science*, *37*, 799–819.

Whitby, E. R., & McMurry, P. H. (1997). Modal aerosol dynamics modeling. *Aerosol Science and Technology*, *27*, 673–688.

Wilson, J., Cuvelier, C., & Raes, F. (2001). A modeling study of global mixed aerosol fields. *Journal of Geophysical Research*, *106*, 34,081–34,108.

Wright, D. L., Kasibhatla, P. S., McGraw, R., & Schwartz, S. E. (2001). Description and evaluation of a six-moment aerosol microphysical module for use in atmospheric chemical transport models. *Journal of Geophysical Research*, *1068*, 20,275–20,291.

Wright, D. L., McGraw, R., Benkovitz, C. M., & Schwartz, S. E. (2000). Six-moment representation of multiple aerosol populations in a sub-hemispheric chemical transformation model. *Geophysical Research Letters*, *27*, 967–970.

Wright, D. L., McGraw, R., & Rosner, D. E. (2001). Bivariate extension of the quadrature method of moments for modeling simultaneous coagulation and sintering of particle populations. *Journal of Colloid and Interface Science*, *236*, 242–251.

Yu, S., Kasibhatla, P. S., Wright, D. L., Schwartz, S. E., McGraw, R., & Deng, A. (2003). Moment-based simulation of microphysical properties in the eastern United States: Model description, evaluation, and regional analysis. *Journal of Geophysical Research*, *108*, 4353.